Publications of the Astronomical Society of the Pacific
109: 725–737, 1997 June

Atmospheric Intensity Scintillation of Stars. II. Dependence on Optical Wavelength

DAINIS DRAVINS, LENNART LINDEGREN, AND EVA MEZEY

Lund Observatory, Box 43, S-22100 Lund, Sweden
Electronic mail: dainis@astro.lu.se, lennart@astro.lu.se, evam@astro.lu.se

ANDREW T. YOUNG

Department of Astronomy, San Diego State University, San Diego, California 92182-1221
Electronic mail: aty@mintaka.sdsu.edu

Received 1997 January 22; accepted 1997 March 3

ABSTRACT. Atmospheric intensity scintillation of stars on milli- and microsecond time scales was extensively measured at the astronomical observatory on La Palma (Canary Islands). Scintillation statistics and temporal changes were discussed in Paper I, while this paper shows how scintillation depends on optical wavelength. Such effects originate from the changing refractive index of air, and from wavelength-dependent diffraction in atmospheric inhomogeneities. The intensity variance σ_I^2 increases for shorter wavelengths, at small zenith distances approximately consistent with a theoretical $\lambda^{-7/6}$ slope, but with a tendency for a somewhat weaker dependence. Scintillation in the blue is more rapid than in the red. The increase with wavelength of autocorrelation time scales (roughly proportional to $\sqrt{\lambda}$) is most pronounced in very small apertures, but was measured up to $\varnothing$ 20 cm. Scintillation at different wavelengths is not simultaneous: atmospheric chromatic dispersion stretches the atmospherically induced "flying shadows" into "flying spectra" on the ground. As the "shadows" fly past the telescope aperture, a time delay appears between fluctuations at different wavelengths whenever the turbulence-carrying winds have components parallel to the direction of dispersion. These effects increase with zenith distance (reaching $\simeq$ 100 ms cross-correlation delay between blue and red at $Z = 60°$), and also with increased wavelength difference. This time delay between scintillation in different colors is a property of the atmospheric flying shadows, and thus a property that remains unchanged even in very large telescopes. However, the wavelength dependence of scintillation amplitude and time scale is "fully" developed only in small telescope apertures ($\lesssim$ 5 cm), the scales where the "flying shadows" on the Earth's surface become resolved. Although these dependences rapidly vanish after averaging in larger apertures, an understanding of chromatic effects may still be needed for the most accurate photometric measurements. These will probably require a sampling of the (stellar) signal with full spatial, temporal, and chromatic resolution to segregate the scintillation signatures from those of astrophysical variability.

1. INTRODUCTION

Extensive and systematic observations of stellar intensity scintillation on short and very short time scales ($\simeq$ 100 ms–100 ns) arising in the terrestrial atmosphere have been made at the observatory on La Palma (Canary Islands). The results make up a series of three papers. Paper I, *Statistical Distributions and Temporal Properties* (Dravins et al., 1997a), analyzed the temporal statistics of scintillation, and its behavior on time scales from microseconds to seasons of the year. The corresponding probability distributions, autocorrelation times, or gradual changes during a night are determined by evolving atmospheric patterns, and are analogous for scintillation at different wavelengths. The present Paper II deals with the more subtle differences that exist, at any time, between scintillation in different optical colors. Paper III, *Effects for Different Telescope Apertures* (Dravins et al. 1997b), will finally evaluate how scintillation manifests itself in telescopes with varying diameter and central obscuration.

That atmospheric fluctuations are not synchronous at all wavelengths can already be seen with the naked eye, by observing twinkling stars low in the sky. Indeed, such observations have inspired expressions such as "like a diamond in the sky," associating with a jewel's flashes of sparkling color. However, the visual perception of chro-

matic scintillation is feasible only at large zenith distances, and applies to the eye's very small aperture ($\simeq$ 5 mm), and limited frequency response ($\lesssim$ 15 Hz).

Closer to the zenith, and for larger telescope apertures, wavelength effects are not striking, and may require fairly accurate measurements for detection. As described in Paper I, the present extensive set of observations (24 full nights), using photon-counting detectors with on-line digital signal processing, indeed did reveal several new details in scintillation properties. Below, we also present some features of its wavelength dependence that do not appear to have been previously documented in the literature. Paper I described the experimental arrangements, and also gave an overview of scintillation mechanisms and phenomena in general.

A number of scintillation phenomena are known, or can be expected, to vary between different optical colors. Most obviously, the refractive index of air changes with wavelength. Scintillation comprises a diffractive component: the diffraction pattern produced from a given inhomogeneity has a different scale at different wavelengths (although their "flying shadows" move with the same windspeed), leading to differences in time scale. Furthermore, intensity fluctuations at different wavelengths are not simultaneous. A time delay between them is caused by atmospheric chromatic dispersion which stretches the atmospherically induced flying shadows into "flying spectra" on the ground. Since scintillation at different wavelengths is not synchronous, its heterochromatic power measured through broader optical bandpasses must be less than its monochromatic value.

One main purpose of this project is to better understand actual (nonideal) scintillation properties at premier observatory sites such as La Palma. Even if the chromatic effects in themselves could appear to be of not especially great magnitude, an improved understanding of their functional dependence and actual behavior will aid in segregating the atmospheric component in accurate astronomical photometry, and in understanding what scintillation modeling is adequate for any given application.

Optimum methods for the most accurate ground-based stellar photometry are yet to be developed. Plausible *passive* systems (see Paper III) could involve time-resolved photometry over the spatially resolved telescopic entrance pupil, simultaneously in several photometric colors. To segregate the signal of astrophysical variability from the atmospheric one would then involve modeling the latter in terms of both its temporal, spatial, and chromatic dependences.

Future *active* systems of second-order adaptive optics are envisioned to correct not only the atmospherically distorted phase, but also the amplitude, reducing or even eliminating effects of scintillation. The scales ($\lesssim$ 5 cm) over which the chromatic effects in scintillation become pronounced are the same ones over which such adaptive optical components must be operated. Obviously, the choice for the (natural or artificial) guide star(s) in such systems must be made knowing whether it will adequately reproduce the behavior at the desired wavelength for the target object.

The atmospheric chromatic dispersion causing "flying spectra" on the ground could even be used to advantage, since the spatial separation of scintillation of different colors implies that atmospheric fluctuations might appear earlier (by perhaps tens of milliseconds) at some particular wavelength than at another, thus providing an early "warning" for an adaptive system to adjust itself for the second wavelength.

The original main motivation, however, is to exploit an improved understanding of actual scintillation properties in order to search for very rapid fluctuations in astronomical objects, such as arising from instabilities in mass flows around compact objects—white dwarfs, neutron stars, or presumed black holes (Dravins 1994). To segregate successfully the possibly quite subtle astrophysical high-speed variability from the superposed atmospheric fluctuations may require a detailed correction for the atmospheric effects.

There exist astrophysical projects which demand a precise calibration of chromatic scintillation. In studying the mass flow in accretion columns, one may wish to observe phase shifts between oscillations in different layers (visible at different wavelengths due to different source opacities). Or, following a stellar flare, one can expect certain time delays between fluctuations in different spectral lines formed in the same deexcitation cascade with photons of different wavelengths emitted almost (but not precisely) simultaneously. Unless the atmospheric phenomena are adequately understood, and corrected for, they could easily be mistaken for astrophysical phenomena. For example, the chromatic effects in "flying spectra" observed away from the zenith produce intensity modulations that move systematically from one end of the spectrum to the other. For actual observing programs, a very real question is how to select the calibration source(s): How close in (average) color and in position on the sky must the scintillation calibration be located in order to permit a compensation of atmospheric phenomena for any given accuracy requirement?

2. CHROMATIC EFFECTS IN SCINTILLATION

2.1 Early Studies

Close to the horizon, color effects in the twinkling of stars are prominent to the naked eye, and already attracted attention a very long time ago. However, until the advent of photoelectric photometry, only rather qualitative studies through visual observations or by photography were possible.

Arago (circa 1850) already employed small oscillations of a small telescope to spread the scintillations into a spatially resolved intensity variation. Montigny (circa 1860) mounted rotating optical elements behind the telescope eyepiece, stretching out the temporal changes of the stellar image into (visually observable) variations along the circumference of a circle. Colors of many hues were observed and the frequency of variation studied. Respighi (circa 1870) built upon these results, using a visual spectroscope. From the behavior of those dark bands that cross the spectrum in chromatic scintillation, he deduced that the angular deviation of luminous rays must be very small, and scintil-

lation must originate at great heights. A review of some of these historic observations is in Monaco (1990).

Somewhat analogous experiments, but with photographic recording, were made by Zwicky (1950) using an objective prism on the 18-in. Schmidt telescope on Palomar. Photographic drift images showed that the light from a star at any instant seldom is "white" but, in any given wavelength range, the apparent brightness may fluctuate by a great amount. Furthermore, the light from the star reaches the observer in a time sequence of colors, sometimes chasing one another along the length of the spectrum. By rapidly moving the telescope, a very high time resolution was achieved, showing that the dark and bright bands follow one another in intervals of 1 ms or less. Like earlier observers, Zwicky noted that the color-intensity patterns are most regular at the zenith and become more irregular closer to the horizon. Related experiments were also made by Ellison and Seddon (1952).

The chromatic effects that are so visible in visual scintillation are prominent only at large zenith distances, and in very small apertures. Closer to the zenith, and in larger telescopes, the power of scintillation becomes nearly independent of wavelength, and may require fairly accurate measurements for detection of color differences. Even with the advent of photoelectric measurements, efforts in finding chromatic effects were often not successful. Thus, despite an extensive measurement program, Protheroe (1955) could only conclude that color effects, if present, cannot be large.

2.2 Differences in Amplitude

At large zenith distances, Zhukova (1958) found scintillation at λ460 nm to be greater than that in white light. However, photographic spectral trails over λ380–580 nm revealed no correlation between variations in different spectral regions (Zhukova 1959). Observing near the zenith through a small aperture, Burke (1970) found the simultaneously measured intensity variance greater around λ420 nm than around 550 nm. Analyzing these data, Young (1970b) concluded that effects of aperture averaging and chromatic dispersion could explain the observed dependence being weaker than the theoretically expected $\lambda^{-7/6}$ relation. Other studies of chromatic scintillation have been by Filippov (1972) and Knoechel and von der Heide (1978).

A more extensive study was made at Mauna Kea (Hawaii) by Dainty et al. (1982). They observed with a small (2.7 cm) aperture at $Z < 40°$, using filters in red, green, and blue. Similar to earlier observations it was found that, while the intensity variance does increase in the blue, measured ratios between σ_I^2 at different wavelengths show a weaker dependence than the $\lambda^{-7/6}$ prediction. As an explanation, the authors suggested some remaining effects from aperture integration.

However, Stecklum (1985) did find an agreement with the $\lambda^{-7/6}$ law at small airmasses, using *uvby* filters through mostly a 2.8 cm aperture. This agreement was not obtained in his first measurements which, with almost 3 min between successive measurements, undersampled the atmospheric variability (cf. Sec. 7 in Paper I). Only after the time between successive measurements had been reduced to 6 sec did the time variability of scintillation statistics appear resolved, and the color dependence now approached the theoretically expected value.

2.3 Differences in Time Scale

Although, at shorter wavelengths, the characteristic variability is expected to occur on shorter time scales, there exist but few previous measurements of this dependence. At Observatorio del Teide on Tenerife (the neighbor island of La Palma), Fuentes et al. (1987) measured scintillation in the *J*, *H*, *K*, and *L* near-infrared atmospheric windows, finding the autocorrelation time to be some 30% longer in $L(\lambda 3.5\ \mu m)$ than in $J(\lambda 1.2\ \mu m)$. Also, the relative variances between pairs of passbands showed consistently less scintillation at longer wavelengths. However, the precise interpretation of these data must account for the wavelength-dependent aperture averaging in their 50-cm telescope, being not very much smaller than the diffraction Fresnel-zone size.

Somewhat related studies exist concerning the wavelength dependence of time scales in seeing, such as speckle lifetimes inside focused stellar images. For different sites, telescopes, and methods, correlation times increase from perhaps 5 ms in the visual (Dainty et al. 1990) to $\gtrsim$ 100 ms in the far-infrared (Selby et al. 1979; Mariotti 1983).

There also exist time-scale measurements in terrestrial scintillation. An arrangement with coincident laser beams traveling over a long horizontal path was used by Dunphy and Kerr (1973) to reveal more rapid fluctuations at λ488 nm than at λ10.6 μm. The application to stellar conditions may be limited here because of saturation effects designed into these experiments.

2.4 Correlations between Different Colors

Manifestations of atmospheric chromatic dispersion (the blue ray is bent more strongly than the red one, so the blue image appears above the red one in the sky) may become visible even to the unaided eye; the best-known example is the "green flash" occasionally seen at sunrise and sunset. Besides the obvious chromatic twinkling of stars, some more subtle effects can also be seen with the unaided eye, such as the time delay between scintillation in different colors at large-zenith distances. If one views a star with the wind direction carrying the "flying-shadow" pattern from one eye to the other, then some correlation may be detected, even if the time delay between the images in different colors is only on the order of 10 ms (Warner 1988).

Since scintillation varies with wavelength, a dependence must exist on the optical bandwidth over which it is measured. Some (unintended) observations of apparent bandpass effects can be found in the literature as some investigators, searching for color effects, obtained inconclusive data, apparently due to the use of broadband filters, where fluctuations in different colors within the passband became decorrelated with increasing zenith distance.

More systematic studies of the bandpass dependence were made by Jakeman et al. (1976), who observed at

$Z = 69°$, using a very small (0.8 cm) aperture. The intensity variance was measured to be much greater (by factors of $\simeq 5$) through a narrow-band filter, as compared to white light.

Since atmospheric dispersion separates the average optical paths of rays in different colors, these intersect a turbulent layer at somewhat different locations. Measurements at multiple wavelengths of single-star scintillation then permit a reconstruction of certain upper-atmosphere inhomogeneities (such as their spatial-correlation functions). Hubbard and Reitsema (1981) used orientable double apertures to study the wind direction and velocity. Their Arizona data include cross-correlation functions between blue and red, the delays reaching $\simeq$ 100 ms for zenith distances $Z \simeq 75°$.

Caccia et al. (1988) measured two-color single-star scintillation at Haute-Provence to study the vertical profile of the refractive-index structure coefficient C_n^2, identifying the presence of several discrete turbulence layers. The two-color method exploits rays at two wavelengths that cast two slightly different shadow patterns on the ground, analogous with double-star measurements (Sec. 9 in Paper I), where each component from a binary star casts a different pattern.

2.5 Solar-Eclipse Shadows

Flying shadows are observed close to solar-eclipse totality, and careful measurements also reveal chromatic effects. Young (1970c) reported observations where, near second contact, the shadow bands (with a contrast of $\simeq$ 3% of the average) were separated by about 6 cm at λ 360 nm and by 8 cm at λ 560 nm. More extensive photoelectric measurements of flying shadows were made by Quann and Daly (1972). The shadow bands were more pronounced in the blue and near-ultraviolet, than in the green/yellow.

The scintillation theory of eclipse shadow bands was formulated by Codona (1986). It predicts the band spacing to decrease as totality nears, becoming progressively more wavelength-dependent with a final spacing proportional to the square-root of wavelength. The contrast becomes λ dependent as diffraction effects become more important near totality, with shadows at shorter wavelengths exhibiting higher contrast.

However, this λ dependence is complicated by the variation of the solar limb darkening with wavelength. That is greater at short wavelengths, making the effective width of the exposed solar crescent narrower, thus increasing the shadow-band contrast.

2.6 Other Effects

Scintillation is not polarized. This was already investigated by Mikesell et al. (1951), who found the fluctuations similar in different planes of (linear) polarization. Also, for eclipse shadow bands, no polarization effects are expected from theory (Codona 1986), and none are observed (Quann and Daly 1972).

Analogous to the discussion in Paper I (Sec. 6.7) on limiting time scales of atmospheric fluctuations in general, there may exist λ-dependent extinction anomalies or similar phenomena over time scales much longer than "ordinary" scintillation. The size of such effects is indicated by extinction variations at Crimea, measured at four wavelengths by Nikonov et al. (1988). With a time resolution of 20 sec, they found amplitudes around 0.01 mag. Although such variations occur simultaneously in all spectral regions, their amplitude increases toward shorter wavelengths.

A certain literature exists about chromatic effects in laser-beam propagation, e.g., about correlations between scintillation at two different wavelengths, measured in laser beams propagating over the same atmospheric path. Thus, with increasing turbulence, Ben-Yosef et al. (1986) and Churnside et al. (1992) found a loss of correlation between scintillation in two colors, at discrepancy with the weak-turbulence theory.

2.7 Present La Palma Observations

As described in Paper I, our observations were made using a 60 cm reflecting telescope in Observatorio del Roque de los Muchachos, at 2360-m altitude on La Palma. For measurements through apertures other than the full one, a rotatable mask enabled rapid changes between circular unobscured apertures of various size. The measuring instrument, QVANTOS Mark I (Dravins et al. 1994), is a computer-controlled high-speed photometer with rapid photomultipliers, and very fast real-time digital signal processors (cycle time = 20 ns).

The Canary Islands experience certain seasonal changes in their weather patterns, and therefore observing campaigns were carried out both in winter (November/December), and in summer (July/August). Out of the total of 24 observing nights spent in measuring various scintillation phenomena, chromatic effects were studied during five nights in winter, and three in summer. Data were recorded alternating through either two, three, or four color filters, repeating the cycle several times during perhaps an hour, before starting a similar sequence with a different telescope aperture. Aperture diameters between ∅ 2.5 and ∅ 60 cm were used.

For studies of color dependences, interference filters centered at wavelengths of λ 400, 500, 550, 600, and 700 nm, with full widths at half-maxima $\Delta\lambda \simeq 70$ nm were used, supplemented by a few narrow-band ones ($\Delta\lambda \simeq 10$ nm) at λ 365 and λ 540 nm. Measurements in "white light" had an effective wavelength extent of $\Delta\lambda \simeq 300$ nm. The filters could be placed in front of either one of the two photomultipliers, or made common to both.

The signal processor was programmed to give either (a) the probability density function (PDF), i.e., a histogram for the number of time intervals (of preselected duration) during which there were recorded exactly 0, 1, 2, 3...63 photon counts; (b) a 64-point temporal autocorrelation (ACO) function in time (with a preselected time-lag interval), or (c) an analogous cross-correlation function (CCO) between the counts from two different photomultipliers. The sample-time duration could be changed in software between 20 ns and 10 sec. Each measurement (integration) lasted for typically 100 sec, and the time between the completion of successive measurements could usually be kept to between

2 and 3 min. For details of the data reduction procedures, see Paper I.

3. MECHANISMS FOR CHROMATIC SCINTILLATION

Following the understanding of the optical physics of scintillation in the 1960's (see Paper I), more quantitative tests and more sophisticated theories became feasible. The early theory by Reiger (1963) was generalized by Young (1969) also to include effects of diffraction and chromatic dispersion. In such a wave-optical treatment, the components of atmospheric turbulence are regarded as phase gratings, and not merely as refracting surfaces.

3.1 Amplitude Dependence

As described in Sec. 4.3 of Paper I, a simple wave-optical model of scintillation predicts the intensity variance σ_I^2 to obey:

$$\sigma_I^2 \propto \lambda^{-7/6}(\sec Z)^{11/6}\int_0^\infty C_n^2(h)h^{5/6}dh \quad (D < r_F), \tag{1}$$

where $C_n^2(h)$ is the refractive-index structure coefficient, h is altitude in the atmosphere, and Z is the zenith distance. Scintillation thus decreases with increasing wavelength λ. This expression assumes that there is no spatial or temporal averaging, i.e., the telescope aperture diameter D must be (much) smaller than the diffraction Fresnel-zone size: $D \ll r_F = \sqrt{\lambda h}$, and the time resolution of the measurements must be correspondingly fine.

Neglecting effects of wave optics, the geometric-optics approximation gives instead:

$$\sigma_I^2 \propto D^{-7/3}(\sec Z)^3\int_0^\infty C_n^2(h)h^2dh \quad (D \gg r_F). \tag{2}$$

This approximation is valid for aperture diameters much greater than the Fresnel-zone size. Then the amount of scintillation is independent of wavelength and merely decreases with increasing D (except for a slight increase to shorter wavelengths, due to the wavelength dependence of the refractivity in air). In case the aperture is neither very small nor very large, the changes with wavelength depend upon the variation of the structure coefficient with altitude h.

The relation between the wave- and geometric-optics cases, and the origins of the $-$ 7/6 power wavelength dependence in the former case may be not very intuitive. However, from the geometric optics relation [Eq. (2)], it emerges by setting the aperture diameter D equal to the diffraction Fresnel-zone size $= \sqrt{\lambda h}$, leading to $[(\lambda)^{1/2}]^{-7/3}$, i.e., $\lambda^{-7/6}$ (Young 1970a).

3.2 Mechanisms for Time-Scale Dependence

As described in Paper I, theories of scintillation often begin with a "phase-changing screen," i.e., a thin slab of turbulent medium that corrugates the incident wavefront. After passage through such a phase screen, the characteristic modulation in the (flying) shadow pattern has a spatial scale of $d \simeq \sqrt{\lambda h}$, which is the Fresnel-zone size r_F. For a star near the zenith, observed through 10 km high turbulence, the value of r_F ranges from 6 cm at λ 350 nm to 9 cm at λ 800 nm. The time scale of scintillation is primarily set by the speed of the flying shadows, i.e., by the winds carrying the atmospheric inhomogeneities.

Although the windspeeds are not coupled to the wavelength of light, the structures in the flying shadows carried by these winds are "finer grained" at shorter wavelengths (i.e., the Fresnel-zone sizes are smaller), and the corresponding scintillation should display more power at higher spatial and temporal frequencies. Also, the dependence on, e.g., aperture size might be slightly different for different wavelengths since the patterns are probably differently influenced by wind-shear averaging. For plots of theoretical (spatial) autocovariance functions and power spectra of stellar shadow patterns, see Roddier (1981; his Chap. 8; and his Figs. 12 and 14).

For idealized conditions, the time scale can be expected to increase with the square root of the wavelength, corresponding to the time the wind needs to carry the turbulence over a Fresnel-zone $r_F = \sqrt{\lambda h}$. In the presence of wind shear, however, the flying-shadow pattern changes on a time scale determined by some typical mean-square difference of the wind speeds in the turbulent layers. This time scale might not be very different from the time for the mean wind to move the pattern of a single layer by a Fresnel-zone size, if the wind directions at different heights differ by a radian or more. This discussion should apply if the scintillation is weak (unsaturated).

At large zenith distances, however, scintillation observed through small apertures may no longer be considered as weak, and nonlinear phenomena enter (effects of successive atmospheric layers become multiplicative rather than additive). Because the probability distribution is closely log-normal, the characteristic time scale given by a simple theory is that of the *logarithm* of the intensity; the time scale of the intensity itself becomes shorter, because of the spikes in the intensity record.

3.3 Causes of Shift between Different Colors

Intensity fluctuations at different wavelengths are not exactly simultaneous, in particular because of atmospheric chromatic dispersion, caused by wavelength changes of the refractive index of air. The "flying shadows" on the ground become chromatic (flying spectra), a projection onto the ground of starlight which has been spectrally dispersed by the atmosphere. The blue part is displaced from the red, but the structure of the shadows remains similar, provided the spectral dispersion has occurred after passage of the relevant turbulence. As the shadows fly past the telescope aperture, a time delay between fluctuations at different wavelengths becomes visible, provided the turbulence-carrying winds have components parallel to the direction of dispersion. (At right angles from this, there is no effect.)

Fluctuations at different wavelengths can also have "intrinsic" differences because chromatic dispersion may have bent rays at different colors to traverse different atmospheric inhomogeneities. At large zenith distances, blue and

red rays can be separately affected by turbulent elements separated by distances comparable to a telescope aperture.

Two rays of wavelengths λ_1 and λ_2, for which the refractive index differs by $\Delta\mu$, will be separated at height h by:

$$dh = \tan Z \sec Z \int_0^h \Delta\mu(h')dh'. \quad (3)$$

Here, $\Delta\mu \tan Z$ corresponds to the angular dispersion and $h \sec Z$ to the distance from the observer. Since $\Delta\mu$ is a function of height, it must be included in the integral. For this discussion, we can approximate $\Delta\mu(h) = \Delta\mu_0 \exp(-h/h_D)$, with the density scale height $h_D \simeq 8$ km. Then the ray separation at the top of the atmosphere becomes (Young 1969):

$$h_\infty = \Delta\mu_0 \tan Z \, h_D \sec Z. \quad (4)$$

The effects of differential refraction become important at larger zenith distances, as rays of different wavelengths traverse appreciably different paths, and hence sample different parts of the turbulent medium. If the chromatic ray separation exceeds the Fresnel-zone size $\sqrt{\lambda h}$, the effect becomes significant. Already early studies of this effect by Montigny, Respighi, and Lord Rayleigh sought to explain the colored twinkling of stars at low altitudes, and the phenomenon has been discussed repeatedly since then (e.g., Tatarskii and Zhukova 1959; Young 1969, 1970b).

The wavelength variation in the refractive index of air is most pronounced at shorter wavelengths. Standard refractivities $(n - 1)$ for the central wavelengths of the filters used in the present project are: $[(n - 1) \times 10^7]$: λ 365 nm–2838; 400–2817; 500–2781; 550–2771; 600–2763; and λ 700–2753. Thus, between blue and red, the index of refraction differs by $\simeq 5 \times 10^{-6}$, a few percent of the refractivity. The total atmospheric refraction at $Z = 45°$ is about an arcmin and the differential refraction $\Delta\mu \tan Z$ between blue and red is a few arcsec. The ray separation between blue and red rays, looking from one point on the ground, at the top of the atmosphere then becomes about 15 cm, increasing to about 40 cm at $Z = 60°$ [Eq. (4)].

There exist further physical parameters which, at least on some accuracy level, will influence scintillation and its wavelength dependence. For example, the indices of refraction for "air" quoted above refer to dry, clean air at a temperature of 15 °C and sea-level pressure. A more detailed analysis would consider the wavelength fluctuations of refractive index also caused by other environmental quantities, such as temperature or humidity. In this case, the functions also describing their power spectra (such as the structure functions for the humidity content of air) would be needed to model precisely the propagation and scintillation of light.

Such considerations become important for studies in the infrared (especially in marine environments), where (besides hydrodynamic turbulence) effects of absorption by water-vapor and other molecules do enter (Kagawa et al. 1993; Schwering and Kunz 1995). The density of water vapor in various atmospheric structures can be modulated by seasonal temperature effects, atmospheric waves, etc. These could be the reasons why the scintillation statistics of far-infrared beams do not obey simple extrapolations of the laws applied in the optical. Even further out in the thermal infrared and the microwave radio, the refractivity of air becomes strongly humidity-dependent, and also effects of atmospheric aerosols and their thermal emission enter.

Wavelength effects are also relevant in scintillation applications such as stellar occultations by turbulent planetary atmospheres. A wave-optical theory of turbulent scintillation in planetary atmospheres is able to deduce quantities such as the cross correlation between fluctuations at two wavelengths (Hubbard et al. 1978).

3.4 Heterochromatic Effects

Given that scintillation depends on wavelength, the monochromatic properties of scintillation must differ from the heterochromatic ones, as averaged over broader bandpasses. Atmospheric dispersion causes the ray paths to traverse different inhomogeneities, and leads to phase delays between different colors. One can view the phenomenon from outside or inside the atmosphere: Looking down, the chromatic separation of an incoming ray spreads the flying shadows into spectra at ground level while, looking up from the telescope, one sees different patches of atmosphere in different colors.

However, even for observations in the zenith, with light of different colors traversing the same path, wavelength effects can be expected. First, with the refractive index (and hence its fluctuating part) being greater at one wavelength than another, the resulting scintillation amplitude is correspondingly larger. Since the refractivity of air varies by only a few per cent, detection of this effect requires correspondingly accurate observations. Perhaps the earliest data with sufficient quality were those by Burke (1970), analyzed by Young (1970b).

Second, as discussed in Sec. 3.2 above, the Fresnel-zone sizes r_F from scintillation at different heights give preferred spatial scales in the flying-shadow pattern, proportional to $\sqrt{\lambda}$. When the shadow patterns get "out of phase" at different wavelengths, their finer details become decorrelated. Thus, in broadband averaging, the high spatial frequencies are weaker than in a monochromatic shadow pattern.

All the above effects combine to average out atmospheric fluctuations; thus scintillation measured through a broadband filter must be weaker than that in a narrow spectral line at the same center wavelength. Unfortunately, there appears to exist no simple mathematical formulation by which to describe heterochromatic effects. The chromatic dispersion is a one-dimensional smearing, while aperture averaging is two dimensional. Since the ray separation due to dispersion (typically a few cm) is comparable to both the Fresnel zone, and small features in many telescope apertures (like central obscurations), we have a set of intermingled effects of comparable magnitude.

3.5 Visual Twinkling

The atmospheric conditions required to model telescopic scintillation (high-level turbulence, windspeeds of

10–30 m s^{-1}, etc.) do not predict especially significant scintillation to be observed in small apertures such as the human eye. When visual twinkling is observed, that is due instead to the turbulent boundary layer with a low wind velocity located close to (a few hundred meters) the observer (Young 1969). In this respect, the best astronomical sites differ markedly from ordinary ones; e.g., on La Palma, visual twinkling is almost not noticeable during good summer conditions, and barely so in winter.

At large zenith distances, the visually observed chromatic twinkling can be quite prominent. A primary reason for its easy visibility is the very small aperture of the eye pupil ($\simeq$ 5 mm). Atmospheric dispersion makes the linear separation of red and violet rays comparable to the eye radius already after traversing some hundreds of meters in air, distances that are comparable with the distance from which the visual scintillation comes. One therefore expects strong visual chromatic scintillation low in the sky, as observed.

4. WAVELENGTH DEPENDENCE OF INTENSITY VARIANCE

4.1 Instrumentation and Measurements

Different filters and a variety of aperture sizes were used. Perhaps the most basic wavelength dependence is that for the amount of scintillation, measured by the variance σ_I^2 of the relative fluctuations in intensity I [σ_I is the rms value of $(I - \langle I\rangle)/\langle I\rangle = \Delta I/\langle I\rangle$, where $\langle\ \rangle$ denotes time average].

As described in Sec. 2.2, this dependence has been previously studied, though its functional form was perhaps not very conclusively determined. As experienced both by Stecklum (1985) and ourselves (Paper I), the main experimental difficulties come not from the smallness of the chromatic effects, but rather from their being easily overwhelmed by continuous atmospheric changes. Furthermore, to isolate the wavelength dependence (and to avoid possibly uncertain effects of aperture averaging), very small apertures (no more than a few cm) must be used, limiting the photon fluxes and the noise levels achievable.

A number of sequences were recorded of Polaris, assuring a constant (but large) zenith distance of $Z \simeq 60°$. However, this constancy of zenith distance turned out not to be any special advantage since the atmospheric changes in any case dominate. A number of other measurements were made closer to the zenith. With a slowly varying zenith distance, effects due to changing airmass could be followed and should not affect the comparison between wavelengths.

The smallness of the chromatic phenomena called for a number of control measurements to exclude the influence of instrumental effects. For example, mapping of the photocathode sensitivity areas for different colors was made, and adjustments made accordingly, to avoid possible effects from wavelength-sensitivity changes or similar optical effects. If there would exist patches of uneven, wavelength-dependent, reflectance changes across the telescope mirror, the effective diameter could be smaller at some wavelength, and the scintillation greater and faster (through the aperture-size dependence). Such effects were excluded by noting how scintillation measures converged toward the same value for small apertures (irrespective of location on the mirror), which would not have been the case, had there been significant inhomogeneities.

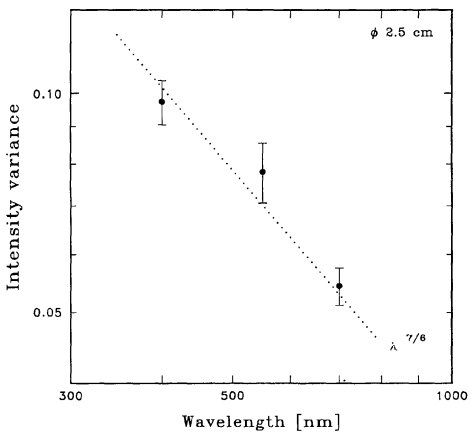

FIG. 1—Wavelength dependence of intensity variance σ_I^2, measured with a 2.5 cm aperture at λ 400, 550, and 700 nm. The theoretically expected slope of − 7/6 from Eq. (1) is marked. The error bars are computed from the full measurement sequence, which is somewhat conservative, since part of the variations is not noise, but rather systematic changes in the atmosphere.

4.2 Results for Different Apertures

At small zenith distances, a systematic wavelength dependence was seen for the smaller (∅ 2.5 and ∅ 5 cm) apertures on all occasions. Within the noise limits, this dependence was found to be approximately consistent with the theoretical $\lambda^{-7/6}$ slope, but with a tendency for a somewhat weaker dependence.

Figure 1 shows the wavelength dependence of the measured intensity variance for a ∅ 2.5 cm aperture. The data are from an hour-long observing sequence of Vega at average zenith distance $\langle Z\rangle = 17°$, during a meteorologically very good summer night. Eight cycles of measurements through filters centered at λ400, 550, and 700 nm were made. Probability distribution functions were recorded with sample times $\simeq$ 290 μs (λ400), $\simeq$ 230 μs (λ550), and 1 ms (λ700), to keep $\langle n\rangle$, the average number of photon counts per sample time, constant $\simeq$ 2.1 (as desired for high-precision differential measurements; cf. Paper I). Some small fraction of the total scintillation was missed by the necessarily finite sample times; since this fraction was slightly greater for the 1-ms sample time at λ700, its true variance should be slightly greater than the point in Fig. 1, further enhancing the tendency of deviation from the $\lambda^{-7/6}$ slope.

The standard errors marked in Fig. 1 originate from the full observational sequence. The error estimates are pessimistic, since part of the variations is not really noise, but rather systematic changes in the atmosphere. These error bars could be somewhat reduced by de-trending the data for such systematic changes. However, in keeping a conserva-

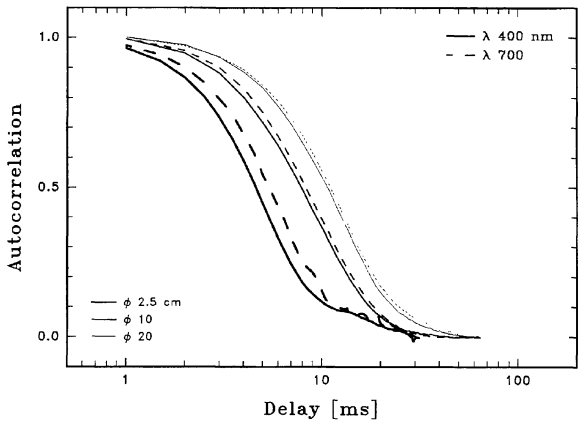

FIG. 2—Autocorrelation functions measured at λ 400 and 700 nm, for different telescope apertures. At shorter optical wavelengths, the fluctuations are more rapid. The effect is most pronounced for the smallest apertures, but could be followed up to ∅ 20 cm.

tive approach, we keep the full error bars here and elsewhere.

As expected [Eq. (2)], the wavelength dependence rapidly diminishes for larger apertures. For $Z \simeq 60°$ in winter, no λ dependence could be identified for apertures larger than 20 cm. Close to the zenith in summer (with a generally smaller intensity variance), the observable λ dependence already disappeared for ∅ 10 cm.

For Polaris at $Z \simeq 60°$, λ dependences such as that in Fig. 1 were consistently observed for both 3.6 and 9 cm apertures, also being somewhat weaker than the theoretical $\lambda^{-7/6}$ prediction. At such larger zenith distances, there is a tendency for the color dependence also to remain visible in somewhat larger apertures. This could be due to the zenith-distance increase of the Fresnel-zone size $r_F = \sqrt{\lambda h}$, as the slant range to the turbulence increases.

This wavelength dependence of intensity variance was incorporated already in the plots of autocovariance and power spectra for different apertures, colors, and seasons (Figs. 14–16 in Paper I).

5. WAVELENGTH DEPENDENCE OF SCINTILLATION TIME SCALES

Systematic studies of the autocorrelation (and autocovariance) functions at different wavelengths, and for several different apertures, were made during a number of nights. Typical measurement sequences involved observations through one aperture at a time, rapidly alternating between two or three different color filters. The autocorrelation half-width was found to increase with wavelength, most pronounced for very small telescope apertures, but possible to follow (with gradually decreasing magnitude) up to ∅ 20 cm: Fig. 2. In parallel, with increasing wavelength, the scintillation power decreases at all frequencies, as already shown in Fig. 16 of Paper I.

The low noise level achieved for Fig. 2 begins to resemble a textbook case. The separation of the curves for the smallest aperture illustrates Fresnel-zone filtering, while the coalescence of the curves for the 20 cm aperture indicates that we are approaching the geometric-optics limit.

Figure 2 shows summer-night measurements of Vega, at moderate average zenith distances $\langle Z \rangle = 28°$ (∅ 2.5 cm); 15° (∅ 10 cm), and 29° (∅ 20 cm). The curves are normalized to unity for a delay equal to one sample-time interval (500 μs or 1 ms). Measurements at λ550 nm fall nicely between those for 400 and 700 nm, but are not plotted in order not to clutter overly the diagram. The measured values for autocorrelation time scales are in Table 1.

The observations involved rapid switching between filters at λ400, 550, and 700 nm; in Fig. 2 the curves for ∅ 2.5 cm are averages from ten such measurement cycles, recorded in 63 min. For ∅ 10 cm, the data are averages of twelve wavelength triplets measured during 90 min, and for ∅ 20 cm, of 16 measurement pairs over 70 min.

A detailed examination of the time evolution of the autocorrelation functions, shows the gross changes mainly to affect the time scale of scintillation, not the shape of the autocorrelation function. For example, although the time scales change, the ratio between $1/e$- and $\frac{1}{2}$- widths remains essentially constant (1.25 ± 0.01). Measurements during different nights gave rather similar and consistent results, summarized in Table 1.

The rightmost column in Table 1 shows the ratio between the time scales at 700 and 400 nm. In the limit of very small apertures and very high temporal resolution, the theory sketched in Sec. 3.2 predicts this ratio to approach the square root of the wavelength ratio $\sqrt{700/400} = 1.32$. Our measurements, however, reach only the value 1.2.

The apparent time variation of the wavelength dependence was monitored during a few nights. It seems that this can be affected by the precise nature of atmospheric changes. The smooth and regular textbook-like wavelength dependence seen in Fig. 2 probably requires developed scintillation with sources high in the atmosphere. By contrast, a sudden incursion of a local, low-level turbulent flow (while perhaps also not very much affecting the magnitude of

TABLE 1

Measured autocorrelation half-widths (ms) for the curves in Fig. 2, and others. The errors given are standard deviations from each full measuring sequence, without any detrending for systematic atmospheric changes. The rightmost column shows the ratio between the time scales at λ 700 and 400 nm.

	λ 400 nm	λ 550 nm	λ 700 nm	(λ 700)/(λ 400)
∅ 2.5 cm (night of Fig. 2)	4.54±0.13	4.95±0.13	5.46±0.17	1.20
∅ 2.5 cm (another night)	4.20±0.25		4.97±0.28	1.18
∅ 5 cm	4.59±0.29	4.85±0.26	5.17±0.43	1.13
∅ 10 cm	8.07±0.20	8.28±0.16	8.42±0.21	1.04
∅ 20 cm	10.96±0.16		11.31±0.23	1.03

scintillation), should not really show any wavelength dependence if the distance to the turbulent layers is so small that the corresponding Fresnel zone $r_F = \sqrt{\lambda h}$ is rather smaller than the telescope aperture. Observed time sequences during some nights did show occasional systematic deviations from the normal wavelength dependence (above apparent measurement-noise levels), which quite possibly may represent such instances of low-level turbulence. Possibly analogous cases were visible in the general changes of scintillation during each night (Fig. 8 of Paper I), where occasional events of increased scintillation amplitude can be identified with incursions of low-level, low-speed turbulence, when it is accompanied by a general increase in scintillation time scale. Such, or analogous, phenomena might account for the wavelength dependence of the time scale and of the variance to be weaker than theoretically expected in an ideal model situation.

6. CROSS CORRELATIONS BETWEEN COLORS

The nonsimultaneity of scintillation in different colors can be measured in their cross-correlation function: a temporal shift between components of "intrinsically" similar scintillation displaces the cross-correlation maximum away from zero time delay. These effects depend on zenith distance, on the upper-atmospheric wind velocity vectors, on the wavelength difference, on telescope aperture size and shape, and probably also other factors.

6.1 Cross Correlation and Cross Covariance

In Sec. 6 of Paper I, the autocovariance ACV (τ) of intensity $I(t)$ for time delays τ was defined (together with a description of its measurement from measured photon counts):

$$\mathrm{ACV}(\tau) = \frac{\langle I(t)I(t+\tau)\rangle}{\langle I\rangle^2} - 1. \qquad (5)$$

We recall that the limiting values for short and long delays are $\mathrm{ACV}(0) = \sigma_I^2$ and $\mathrm{ACV}(\infty) = 0$. The autocorrelation function $\mathrm{ACO}(\tau) = \mathrm{ACV}(\tau)/\mathrm{ACV}(0)$ equals unity at delay zero.

Already for Paper I, this function was occasionally measured in a cross-correlation mode, taking the signals from different detectors which sensed the same signal following a beamsplitter. Now we are introducing cross-correlation and cross-covariance functions between different signals, viz. those of scintillation in different colors.

Relevant measures include the time delay between scintillation seen in, e.g., blue and red. That will be visible as a time lag of the maximum in the cross correlation between scintillation at λ_1 and λ_2. However, such a time lag only affects a certain fraction of the total scintillation power present at either wavelength. This amount of "cross power" that remains correlated between λ_1 and λ_2 is given by the cross-covariance function.

The cross-covariance $\mathrm{CCV}(\tau)$ between $I_1(t)$ and $I_2(t)$, at the wavelengths λ_1 and λ_2, for time delays τ, is defined as:

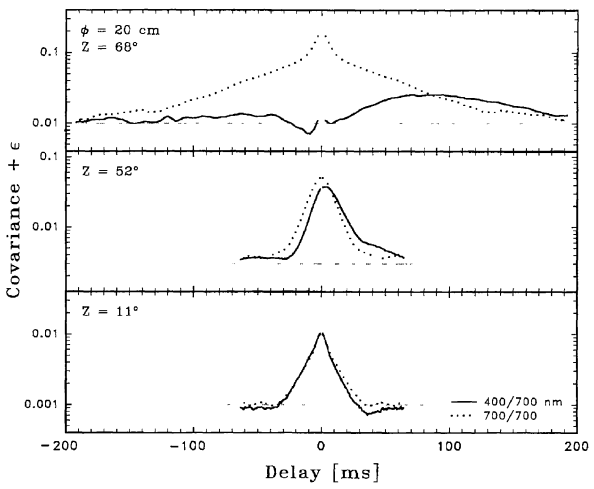

FIG. 3—Cross covariance between intensity fluctuations at λ 400 and 700 nm, measured with a 20 cm diameter aperture, and its zenith-angle dependence. Near the zenith the fluctuations are simultaneous, but with increasing Z a time delay develops, seen as a difference from the (symmetric) autocovariance function for λ 700 nm. The effect is due to atmospheric dispersion, which stretches the "flying shadows" into "flying spectra" on the ground. To enable a logarithmic plot format, and also show the smaller detail, the quantity plotted is the covariance *plus* a small number (ϵ = 0.01, 0.003, and 0.001, respectively); the actual zero level is marked by dotted lines in each panel.

$$\mathrm{CCV}(\tau) = \frac{\langle I_1(t)I_2(t+\tau)\rangle}{\langle I_1\rangle\langle I_2\rangle} - 1. \qquad (6)$$

The corresponding cross-correlation $\mathrm{CCO}(\tau)$ is normalized to show the relative amount of correlation between I_1 and I_2. It may take on values between one (complete correlation), through zero (no correlation), to minus one (complete anticorrelation).

Normally, $\mathrm{CCV}(-\tau) \neq \mathrm{CCV}(\tau)$, so it must be measured for both positive and negative delays (unlike autocorrelation, which is symmetric in τ). Since our signal processor cannot implement negative delays (which would indeed require a clairvoyant detector), pairs of successive measurements were made, switching between the two detectors. Such an exchange between λ_1 and λ_2 is equivalent to a switch of the time axis, i.e., then $\mathrm{CCV}_{12}(-\tau) = \mathrm{CCV}_{21}(\tau)$. These measurements were intermingled with measurements of autocorrelations for each of the signals, also providing measures of $\sigma_I^2(\lambda_1)$ and $\sigma_I^2(\lambda_2)$.

These sets of data, reducing the ACVs and CCVs together in groups, are adequate for calculating various cross dependences. As described in Paper I, our measured correlation functions are clipped ones, in order to simplify the signal processing. While not really constraining the types of analyses possible, this circumstance, together with the necessarily sequential nature of measurements, does require a certain attention to data-analysis procedures since a blind computation of the cross covariances is not uniquely feasible. The method used (for the data in Figs. 3, 4, and 5) involved first an exact solution for the two extreme cases (a) zero cross correlation [$\mathrm{CCO}(\tau) \equiv 0$] and (b) complete

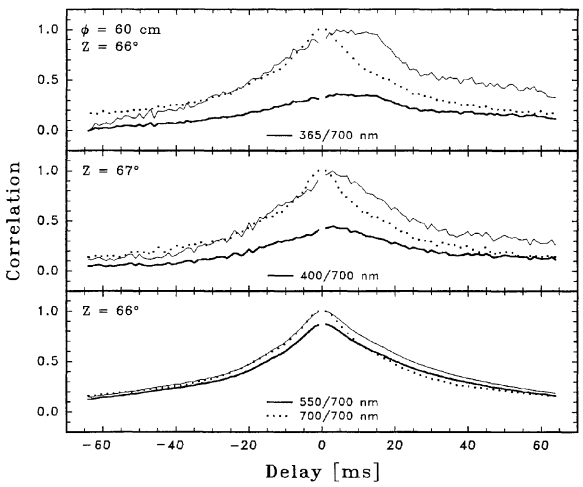

FIG. 4—Cross correlations of atmospheric intensity scintillation between different pairs of colors. The time delays that develop at larger zenith angles depend upon the difference in wavelength. Here, scintillation at λ 700 nm. was successively cross correlated with that simultaneously measured at λ 550, 400, and 365 nm. With increasing wavelength difference (a) the "agreement" (i.e., degree of correlation) between scintillation in different colors decreases, and (b) the time delay increases, visible as a shift of the correlation maximum. In the violet, the dispersion of air changes rapidly with wavelength, which explains the significant differences between the nearby wavelengths of 365 and 400 nm. The functions were normalized to unity for zero delay of the λ 700 nm autocorrelation, and the bold solid curves show the relative power in the cross correlation. The thin solid curves show the cross correlation normalized to unity at its maximum (similar to the autocorrelation), thus more clearly revealing the magnitude of time displacement.

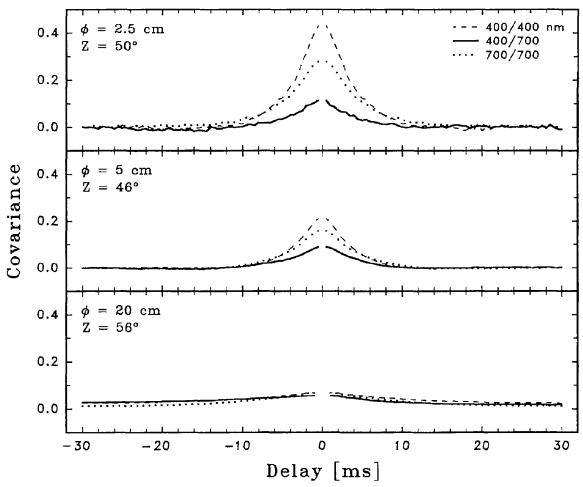

FIG. 5—Cross covariance between intensity fluctuations at λ 400 and 700 nm in the same region of the sky, and its dependence upon aperture size. While the amount of temporal lag between colors (Fig. 3) is a property of the atmosphere, and independent of the size of the telescope, the magnitude of the cross covariance (solid curve) changes with telescope size, and is most pronounced in small apertures ($\lesssim$ 5 cm). Dashed curves show the autocovariance at λ 400 nm; dotted curves at 700 nm. This wavelength difference largely vanishes in greater apertures.

cross correlation [CCO(τ) $\equiv$ 1], and then a scaling of actually measured data to intermediate values. The detailed data handling is closely connected to our specific signal processor used, and will not be further discussed here. A number of tests and simulations of the data reductions indicate that the approximations used should not introduce more errors than perhaps a few percent of the full cross-correlation amplitude, and in any case rather smaller than the noise from atmospheric changes.

6.2 Dependence on Zenith Angle

Near the zenith, the fluctuations in different colors are simultaneous, but with increasing zenith angle, a time delay may develop: Fig. 3. These summer measurements were made along one particular azimuth direction in the sky where the flying-shadow motion had a significant component along the direction of atmospheric chromatic dispersion.

In Fig. 3, the data for $\langle Z \rangle$ = 68° are observations of λ Sco. The curves are averages from two cycles of measuring [autocorrelation at λ_1]-[cross correlation λ_1/λ_2]-[cross correlation λ_2/λ_1]-[autocorrelation at λ_2]. Each correlation measurement lasted 120 sec, using a sample time = 3 ms; the full sequence was covered in 18 min. The time delay of the cross-correlation peak is on the order of 100 ms, a time scale that is an order of magnitude greater than other characteristic time scales in scintillation.

For the smaller zenith distances, the object was Vega. For $\langle Z \rangle$ = 52°, the data are two cycles of correlation measurements of 100 sec each, sample time = 1 ms; full sequence in 21 min. The data for $\langle Z \rangle$ = 11° are averages from three such cycles, covered in 25 min. The [angular] seeing at this later time was noted to be "rather poor."

The asymmetry between positive and negative delays seen in Fig. 3 is a way to determine the actual wind vector, and resolve the 180° ambiguity otherwise inherent in measurements with single telescope apertures. The blue ray is bent more strongly than the red one, so the blue image of the star lies above the red one in the sky. When looking into the wind, each turbulent element crosses the red (lower) ray before it gets to the blue (upper) one, so each wiggle appears in the red scintillation record first. Looking downwind, the reverse holds. This asymmetry is pronounced in the top panel, where the zenith distance is big enough to give good chromatic ray separation. Most of the asymmetry originates in the uppermost layers of the atmosphere, where the ray separation is greatest.

For a numerical estimate of the chromatic ray separation (cf. Sec. 3.3), we note that at Z = 52° (middle panel in Fig. 3), the ray separation for a turbulent region some 10 km above the observatory (15 km slant range) is on the order of 10 cm, increasing to about 30 cm at Z = 68° (top panel), now greater than the 20 cm aperture used. The striking difference between the upper two panels of Fig. 3 is due to the ray separation in one case being smaller than the aperture size, and in the other case, larger.

For Z = 68°, the cross-covariance peaks around 100 ms; if the ray separation is 30 cm, the inferred projected wind speed is 30 cm/100 ms = 3 m s^{-1}. To deduce the full windspeed requires multiplications by factors correcting the geometric projection effects: a zenith-distance factor sec Z, and a wind-azimuth factor sec θ (cf. Sec. 8 in Paper I).

Then estimates of the full windspeed come out as $10-20\ \mathrm{m\ s^{-1}}$, values consistent with other determinations (Paper III).

Some further effects are also visible in Fig. 3. At large zenith distances, the cross-covariance peak is much broader in time delay than the autocovariance peak. One effect must be that, as the two colored beams overlap less and less, contributions to the cross-covariance function come mainly from those turbulent elements that are large enough still to encompass *both* the blue and red rays. At the same time, since only a certain fraction of the turbulence spectrum is involved, the total cross power decreases.

6.3 Dependence on Wavelength Difference

Due to the wavelength changes of the refractive index in air, the "flying shadows" are stretched into "flying spectra." Thus, the amount of delay between scintillation in different colors depends on the wavelength baseline between the colors. In the violet, the dispersion of air changes rapidly with wavelength, and there significant effects may already be seen between nearby wavelengths.

The measurements for Fig. 4 originate from a summer night, observing λ Sco with a ∅ 60 cm aperture, sampling the correlations at 1 ms, and integrating each measurement for 100 sec. The top panel (λ 365/700) has data from one measurement cycle such as described for Fig. 3, recorded during 7 min. Data in the middle panel (λ 400/700) are averages from two such cycles during 15 min, while the λ 550/700 data at bottom come from one cycle of 7 min. The optimum length of integration is not obvious: a larger number of measurements decreases random measurement noise, but increases the variability due to atmospheric changes. Intensity variances σ_I^2 measured in these sequences were: Top panel: λ 365 nm–0.0174; 700 nm–0.0169; Middle panel averages: 400 nm–0.0189; 700 nm–0.0176; Bottom panel: 550 nm–0.0163; 700 nm–0.0140.

As seen in Fig. 4, the cross correlations obviously get more and more different from the autocorrelation, the more the wavelengths differ. Again we see the broadening of the cross correlation as the ray separation increases, just as in Fig. 3. But even at λ 365 nm, the ray separation at the top of the atmosphere does not exceed the 60 cm aperture. The rather mild time asymmetry seen for λ 400/700 nm (compared to that in Fig. 3) suggests that, at this particular time, we were looking at a large angle to the wind azimuth.

6.4 Dependence on Aperture Size

Increasing the telescope aperture causes more extensive averaging of atmospheric fluctuations, and washes out effects from small-scale chromatic structures in the flying shadows: Fig. 5.

The data in Fig. 5 originate from a summer night's observations of Vega. For the smaller ∅ 2.5 and ∅ 5 cm apertures, sample times of 500 μs were used, integrating for 100 sec; the data plotted are averages from two measurement cycles as described for Fig. 3, recorded during some 20 min each. The otherwise equivalent data for ∅ 20 cm had sample time = 1 ms. The particular measurements for ∅ 20 cm were probably somewhat affected by drifting clouds, which could explain the somewhat irregular curve shapes in the bottom panel. As in previous cases, the main limit in the clarity of data is not random noise, but rather atmospheric changes over time. Average (rms) intensity variances $\langle \sigma_I^2 \rangle$ measured in these sequences were: ∅ 2.5 cm (top): λ 400nm—0.430; 700 nm–0.278; ∅ 5 cm (center): 400 nm–0.209; 700 nm–0.158; ∅ 20 cm (bottom): 400 nm–0.068; 700 nm–0.068.

At this particular occasion, not much of an asymmetry or time lag between different colors is visible. Probably, at this particular epoch, we were nearly looking at right angles to the flying-shadow velocity vector, a situation when no time asymmetry would be expected at all. Thus, the different observing epochs for Figs. 3, 4, and 5 demonstrate (besides the other dependences they are illustrating), how chromatic phenomena in scintillation also sensitively depend on azimuth. Obviously, this has implications for the possible choice of standard stars for scintillation calibration.

7. DIFFERENT OPTICAL BANDPASSES

That scintillation changes with wavelength implies that there must exist a dependence on the optical bandwidth over which it is measured (at least as a second-order effect). For example, the monochromatic contrast in the flying shadows must be higher than in "white light," and the intensity variance correspondingly greater.

Although bandpass effects are expected to be more visible near the horizon, and especially for smaller apertures (Young 1970b; Jakeman et al. 1976), we observed at small and moderate zenith distances instead, because the effects there (though smaller) are more relevant to observing programs searching for astrophysical variability. Probability distributions and autocorrelations were recorded, rapidly alternating between narrow band ($\Delta\lambda \simeq 10$ nm), broadband ($\Delta\lambda \simeq 70$ nm), and white light ($\Delta\lambda \simeq 300$ nm), all centered on approximately the same effective wavelength (λ 550 nm). Measurements were made both in winter and in summer, and using apertures of several different sizes. However, no bandwidth dependence above the noise limit (typically a few percent of the intensity variance) could be identified, neither in scintillation amplitude nor time scale.

The primary experimental limitation (also) here comes from the absence of strictly simultaneous measurements: even if these were closely intermingled, successive data records could not be separated by less than a minute or so. Despite several tens of measurement cycles, intrinsic short-term changes of the atmosphere still dominate the errors. Furthermore, to avoid subtle instrumental effects from changing count rates (Appendix of Paper I), neutral-density filters were used to compensate the changing flux through filters of different widths. There are limits to how precisely such compensations can be made; even if the atmospheric changes had been fully resolved, this would likely set a second observational limit.

The conclusion is that, for moderate zenith angles, such effects will not become significant unless scintillation corrections to accuracies better than $\simeq$ 1% of its intensity variance are aimed at.

8. CONCLUSIONS AND OUTLOOK

Analogous to the spatial and temporal structure of scintillation (Paper I), the wavelength dependence is fully revealed when sampled through small telescope apertures ($\lesssim 5$ cm), i.e., on scales where the "flying shadows" on the Earth's surface are largely resolved.

Although chromatic effects in scintillation amplitude and time scale rapidly vanish after averaging in larger apertures, their application will probably still be required to enable very accurate astronomical measurements. Efforts by many have shown that one does not reach the accuracies desired for critical photometric tasks (e.g., studying stellar oscillations or exoplanet transits) by simply 'averaging away' the atmosphere in collecting stellar flux over a large telescope mirror. To perform superior photometry through the atmosphere will probably require systems where the photometric signal is sampled with sufficient spatial, temporal and chromatic resolving power to reveal all their scintillation dependences, and use these as constraints in the fitting of data, thus separating astrophysical variability from atmospheric effects. That the fitted scintillation signal must also obey a chromatic dependence adds another constraint to such systems, correspondingly lowering the noise. Issues about how scintillation appears in different telescope apertures will be further discussed in Paper III.

However, some chromatic effects are inherent to the atmospheric flying shadows and remain independent of telescope size. This applies in particular to the time delay between scintillation in different colors. On one hand, the total scintillation cross power, in which this effect appears, decreases strongly in larger telescopes but, on the other hand, their light-gathering power permits more precise photometry where such effects could still be detected.

Although our current measurements, and those in Paper I did reveal a number of small (though statistically significant) deviations from the predictions of the ordinary Kolmogorov model for atmospheric turbulence, in general there is a quite close agreement. The more precise measurements now available could therefore be taken as a general support for this model. Sources of discrepancy could be connected with the model primarily predicting properties of the logarithm of the intensity, not the intensity itself (e.g., for log-normal statistics, the characteristic time scale for I is shorter than that for $\log I$ because of the temporal spikes in intensity). Other discrepancies could probably be explained by the nonideal and complex atmospheric behavior.

Significant improvements desired for future scintillation studies include the *strictly simultaneous* measurement of different parameters (to avoid effects of atmospheric changes), and the simultaneous use of more than one telescope. Especially the cross-correlation effects depend on the wind velocity vector(s), and thus both on zenith distance and azimuth angle. Given the nature of atmospheric changes, data sets from only one telescope (such as in the present work) naturally have limitations in their achievable sky coverage.

Other challenges for future studies lie in the actual time-resolved imaging of the two- (or perhaps even three-) dimensional flying-shadow patterns on the ground. This could be achieved by imaging the illumination patterns of the telescope entrance pupil (or perhaps even throughout a volume surrounding it), with a spatial resolution of millimeters, and in different colors. Subsequent analyses of such patterns would further clarify the behavior of many scintillation phenomena, which up to now have been sampled only in one temporal dimension. Quite possibly, such analyses will have to be made in parallel with the design of higher-order adaptive optics systems.

This study is part of the High-Speed Astrophysics Program at Lund Observatory, supported by NFR, the Swedish Natural Science Research Council. The QVANTOS instrument development was supported also by FRN, the Swedish Council for Planning and Coordination of Research. At Lund Observatory, we thank in particular research engineers H. O. Hagerbo, B. Nilsson, and T. Wiesel for their highly competent work on various electronic units. The observations were made at The Research Station for Astrophysics on La Palma (Royal Swedish Academy of Sciences), which is part of the Observatorio del Roque de Los Muchachos of the Instituto de Astrofisica de Canarias. Their staff is thanked for valuable help during our several visits there. Parts of the material for this paper were prepared by D. Dravins during a visitorship stay at European Southern Observatory in Garching.

REFERENCES

Ben-Yosef, N., Goldner, E., and Weitz, A. 1986, Appl. Opt., 25, 3486
Burke, J. J. 1970, JOSA, 60, 1262
Caccia, J.-L., Vernin, J., and Azouit, M. 1988, Appl. Opt., 27, 2229
Churnside, J. H., Lataitis, R. J., and Wilson, J. J. 1992, Appl. Opt., 31, 4285
Codona, J. L. 1986, A&A, 164, 415
Dainty, J. C., Levine, B. M., Brames, B. J., and O'Donnell, K. A. 1982, Appl. Opt., 21, 1196
Dainty, J. C., Northcott, M. J., and Qu, D. N. 1990, J. Mod. Opt., 37, 1247
Dravins, D. 1994, ESO Messenger, No. 78, 9
Dravins, D., Hagerbo, H. O., Lindegren, L., Mezey, E., and Nilsson, B. 1994, in Instrumentation in Astronomy VIII, ed. D. L. Crawford and E. R. Craine, Proc. SPIE, 2198, 289
Dravins, D., Lindegren, L., Mezey, E., and Young, A. T. 1997a, PASP, 109, 173 (Paper I)
Dravins, D., Lindegren, L., Mezey, E., and Young, A. T. 1997b, PASP, in preparation (Paper III)
Dunphy, J. R., and Kerr, J. R. 1973, JOSA, 63, 981
Ellison, M. A., and Seddon, H. 1952, MNRAS, 112, 73
Filippov, Yu. K. 1972, Astrometr. Astrofiz. (Kiev), 17, 108
Fuentes, F. J., Fuensalida, J. J., and Sanchez-Magro, C. 1987, MNRAS, 226, 769
Hubbard, W. B., Jokipii, J. R., and Wilking, B. A. 1978, Icarus, 34, 374
Hubbard, W. B., and Reitsema, H. J. 1981, Appl. Opt., 20, 3227
Jakeman, E., Pike, E. R., and Pusey, P. N. 1976, Nature, 263, 215
Kagawa, N., Wada, O., and Koga, R. 1993, Waves Random Media, 3, 317
Knoechel, G., and von der Heide, K. 1978, A&A, 67, 209
Mariotti, J. M. 1983, Opt. Acta, 30, 831

Mikesell, A. H., Hoag, A. A., and Hall, J. S. 1951, JOSA, 41, 689
Monaco, G. 1990 MSAIt, 61, 819
Nikonov, V. B., Bondar, N. I., and Bukach, A. B. 1988, Bull. Crimean Astrophys. Obs., 79, 104 (Izv. Krymskoi Astrofiz. Obs., 79, 111
Protheroe, W. M. 1955, Contrib. Perkins Obs. (University of Ohio) Ser. II, No. 4, p. 28
Quann, J. J., and Daly, C. J. 1972, J. Atmos. Terr. Phys., 34, 577
Reiger, S. H. 1963, AJ, 68, 395
Roddier, F. 1981, Progr. Opt., 19, 281
Schwering, P., and Kunz, G. 1995, in Atmospheric Propagation and Remote Sensing IV, ed. J. C. Dainty, Proc. SPIE, 2471, 204
Selby, M. J., Wade, R., and Sanchez Magro, C. 1979, MNRAS, 187, 553
Stecklum, B. 1985, Astron. Nachr. 306, 145
Tatarski, V. I., and Zhukova, L. N. 1959, Dokl. Akad. Nauk SSSR, 124, 567
Warner, B. 1988, High-Speed Astronomical Photometry (Cambridge, Cambridge University Press)
Young, A. T. 1969, Appl. Opt., 8, 869
Young, A. T. 1970a, JOSA, 60, 248
Young, A. T. 1970b, JOSA, 60, 1495
Young, A. T. 1970c, Sky and Telescope 40, 242
Zhukova, L. N. 1958, Izv. Glavn. Astron. Obs. (Pulkova), Leningrad, 21, No. 162, 72
Zhukova, L. N. 1959, SvA, 3, 533 (AZh, 36, 548)
Zwicky, F. 1950, PASP, 62, 150